17th World Conference on Earthquake Engineering, 17WCEE
Sendai, Japan - September 13th to 18th 2020

STUDY OF THE SOIL FAILURE MECHANISM AT PALU, INDONESIA DURING THE 2018 SULAWESI EARTHQUAKE

A. Dwianca[(1)], S. Rajasekharan[(2)], M. Irsyam[(3)(4)], K. Nakamura[(5)], M. Tonagi[(6)], M.Tanjung[(7)], R. Mikhail[(8)], A. Himawan[(9)], A.Kartawiria[(10)]

[(1)] *Engineering consultant, Kozo Keikaku Engineering, Inc., archeilia-dwianca@kke.co.jp*
[(2] *Engineering consultant, Kozo Keikaku Engineering, Inc., shanthanu-rajasekharan@kke.co.jp*
[(3)] *Head Organization, Indonesian Society for Geotechnical Engineering (HATTI), masyhur.irsyam@yahoo.co.id*
[(4)] *Professor, Bandung Institute of Technology; Faculty of Civil and Environmental Engineering, masyhur.irsyam@yahoo.co.id*
[(5)] *Manager, Kozo Keikaku Engineering, Inc., kengo@kke.co.jp*
[(6)] *Engineering Consultant, Kozo Keikaku Engineering, Inc., tonagi@kke.co.jp*
[(7)] *Researcher, Ministry of Public Work and Public Housing, mahdian_ebrahim@yahoo.com*
[(8)] *Assistant lecturer, Bandung Institute of Technology; Faculty of Civil and Environmental Engineering, reguel.m.hutabarat@gmail.com*
[(9)] *Member, Indonesian Society for Geotechnical Engineering (HATTI), ahimawan74@gmail.com*
[(10)] *Member, Indonesian Society for Geotechnical Engineering (HATTI), andikartawiria@yahoo.com*

Abstract

The 2018 Sulawesi earthquake caused widespread damage in various parts of the Sulawesi island in Indonesia. Among the regions that suffered, Balaroa, a village in Palu which is located 500 meters away from the main Palu-Koro strike-slip fault had undergone extensive damage due to liquefaction and landslide. This paper involves the study on the soil failure mechanism at Balaroa, using data obtained from post-earthquake site investigation and seismic ground response analysis. Firstly, the frequency characteristics of the earthquake wave motion and local site amplification are analyzed. Seismic ground response analysis of the ground is performed using SuperFLUSH 2D, a frequency domain based finite element analysis program. Liquefaction vulnerability analysis of the ground is performed. Good correlation was obtained between the analysis results and the post-earthquake ground profile. The analysis results between 1-D and 2-D soil response analysis are compared. Finally, the possibility of slope failure of the ground is also checked though slope stability analysis of the critical section of the ground surface. The soil failure mechanism is predominantly due to liquefaction. Through the current study, it can be observed that a realistic judgement of liquefaction failure can be obtained through seismic soil response analysis, even using limited soil investigation data.

Keywords: 2018 Sulawesi Earthquake; soil failure mechanism; liquefaction; slope stability; Super-FLUSH

1. Introduction

On 2018, due to the movement of the Palu-Koro strike-slip fault, a series of earthquakes, which included a main shock of magnitude 7.5 earthquake, hit Palu city in the island of Sulawesi, Indonesia Fig. 1. The earthquake tremor caused building to collapse, liquefaction and landslides in multiple regions in Palu, causing widespread damage to human lives and properties. Among the regions that suffered, Balaroa, a village in Palu which is located 500 meters away from the main fault, had undergone extensive damage due to liquefaction and landslide.

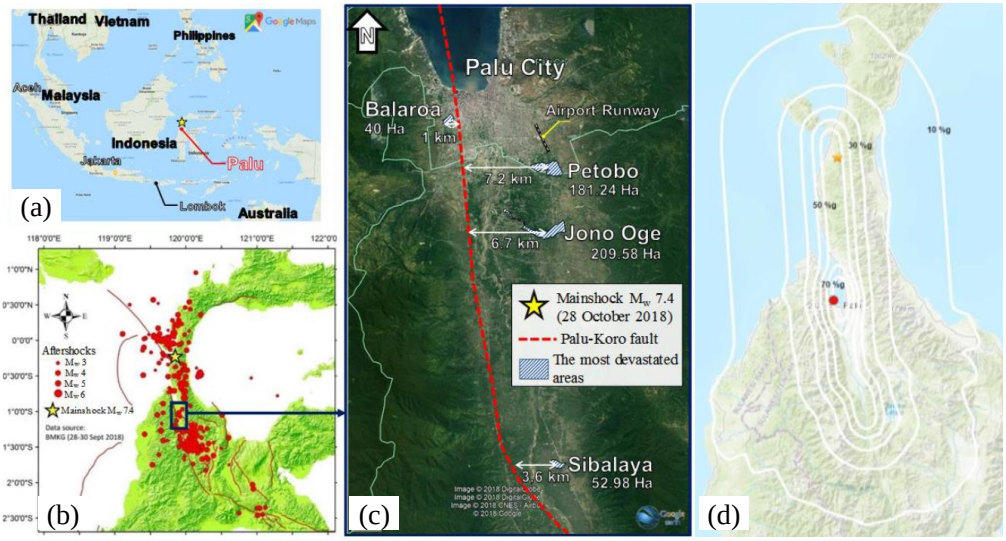

Fig. 1 (a) Location of Sulawesi island (b) Main shock and aftershock distribution [5](c) Palu-Koro fault and Balaroa location (d) wave dispersion and attenuation contour [9]

The soil failure mechanism is attributed to the combination of liquefaction failure and landslide [1]. The current study aims to understand the mechanism of soil failure at Balaroa, through seismic soils response analysis. The numerical simulations are performed using the program SuperFLUSH 2D [2] a frequency domain based finite element analysis program.

The first part of the paper discusses the data obtained from the post-earthquake survey of the region, which is used in the seismic soil response analysis. The data includes the acceleration time history of the strong ground motion recorded during the earthquake, the post-earthquake soil boring data and the ground profile before/after the earthquake. The second part of the paper studies the local soil conditions to understand its frequency and local site amplification characteristics through 1-D modelling of the soil strata. Since the recorded strong motion accelerogram is at ground level, the earthquake wave is de-convoluted to the engineering bedrock level and rotational transformation is applied to the wave motion to obtain the input earthquake wave motion along the failure ground surface direction. The third section discuss the soil modelling and the material properties used for the 1-D and 2-D soil response analysis.

Liquefaction analysis is performed using the data obtained from both 1-D and 2-D ground response analysis. The safety factor against liquefaction is calculated across the model, which is vital in understanding the critical regions of liquefaction. The data obtained from the numerical simulations are compared with site observations. In order to check the influence of landslides/slope slippage, slope stability analysis is performed on predetermined critical slope profiles. Finally, the key results from the current study are highlighted.

2. Post-Earthquake Survey

2.1 Study area

During the 2018 Sulawasi earthquake, approximately 40 hectares of ground was damaged at Balaroa [1]. Although there were other regions that were affected by the earthquake, the current study will focus on Balaroa region due to its proximity Palu-Koro strike-slip fault and the availability of post-earthquake survey data. The strong motion data was recorded in PCI-Palu station [6]. After the earthquake, borehole investigation was performed at three location viz. BH-01 BH-02 BH-03. The data locations are shown in Fig. 2.

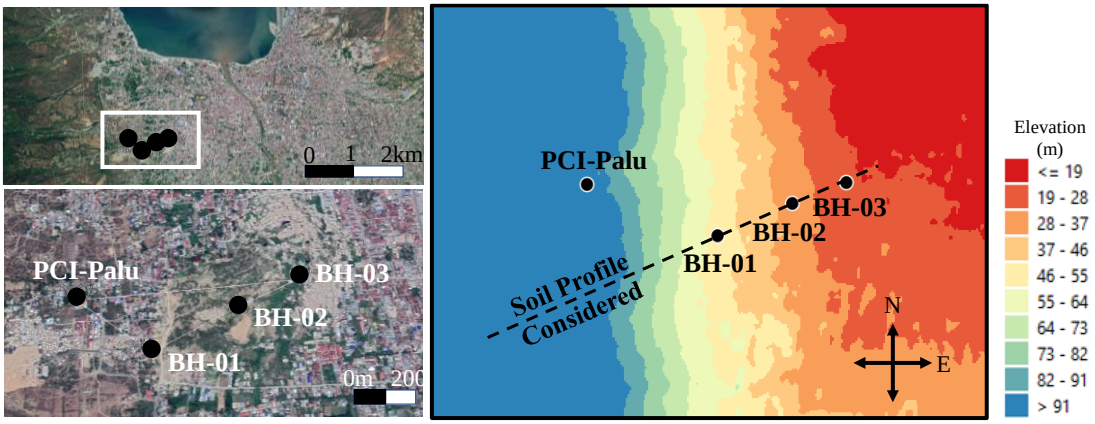

Fig. 2 Location of the data observations stations and the elevation contour of study area

2.2 Earthquake wave characteristics

The earthquake wave motion was obtained from the strong motion sensor located at PCI-Palu station on September 28th, 2018, around 10:02 am. The recorded acceleration time history is shown in Fig. 3. The peak ground acceleration (PGA) was observed to be 281 gal, 203 gal, 335 gal in the East-West (EW), North-South (NS) and Vertical (UD) direction respectively [6]. The response spectrum of the raw wave data is shown in Fig. 3, with an assumed damping ratio of 5%. The response range is predominantly in the time period range of 0.05 sec to 10 sec (0.1 Hz -20Hz). Fig. 5, shows the Fourier spectrum of the three waves normalized with the maximum of each response. A band pass filter between 0.1Hz-50Hz and smoothing window is applied to the raw wave data to plot the Fourier spectrum.

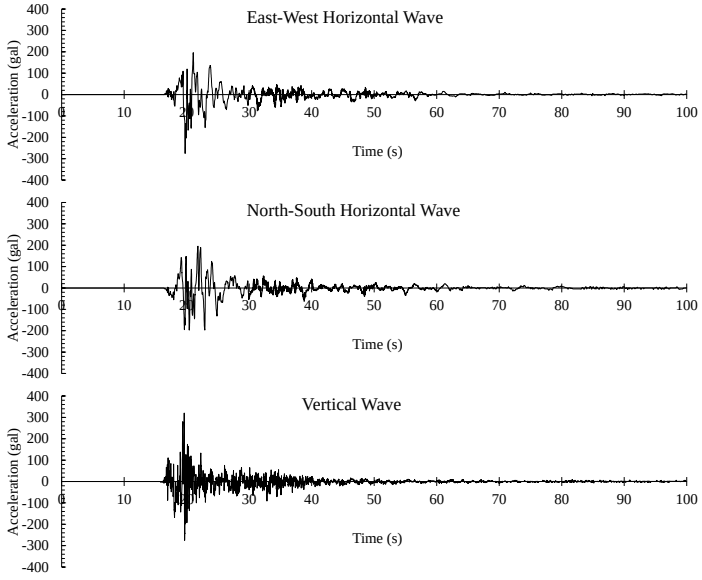

Fig. 3 Recorded strong motion accelerogram during the 2018 Sulawesi Earthquake

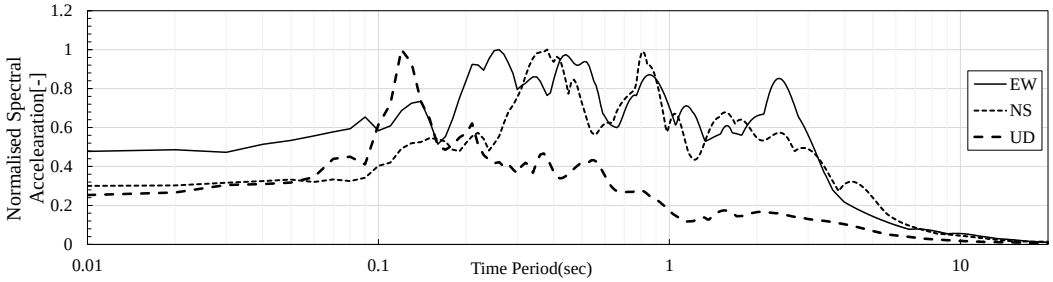

Fig. 4 Normalized Acceleration Response Spectrum of the recorded earthquake wave

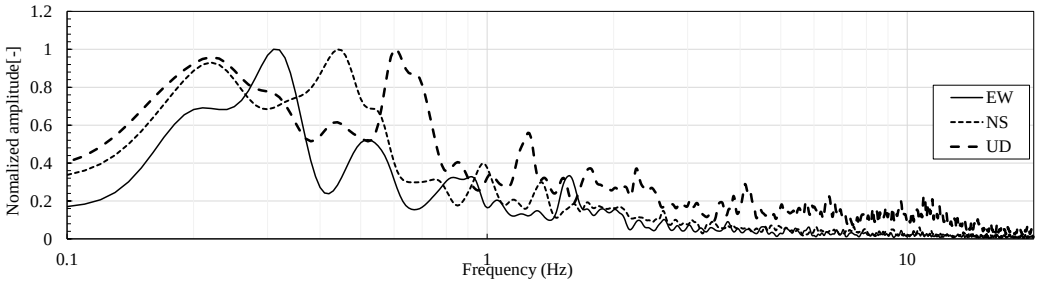

Fig. 5 Normalized Fourier spectrum of the recorded earthquake wave

2.3 Borehole investigation

The borehole investigation was performed at three locations namely BH-01, BH-02 and BH-03, which are carefully picked to represent the damaged area, as a part of the post-earthquake site investigation. The results from the Standard Penetration Test (SPT) performed at these three locations are summarized in Table 1. The boring test was performed up to 30m depth with an aim to compute the Vs30 values of the region. Evidently, the major part of topsoil layer in the region consists of loose sand with a low N value, until around 6m depth.

Table 1 – Boring data at the three stations; Averaged (SPT)-N values and Soil classification

Depth (m)	Borehole BH01		Borehole BH02		Borehole BH03	
	N	Soil Type	N	Soil Type	N	Soil Type
0	2	Very Loose fine Sand with boulder	8	Loose sand with gravel	6	Loose sand with gravel
1.55						
3.55	>50	Boulder	4	Loose sand		
5.55	8	Loose fine sand	9	Medium stiff to stiff silt		
6	100	Boulder				
7.5			52	Hard silt and gravel		
8					6	Soft to medium stiff Clay
9.5			13	Medium dense sand	18	Medium dense Clay
11.5	19	Medium dense sand with gravel	9	Loose fine sand	19	Medium dense Sand
13.3	>50	Granite				
13.5	11	Medium dense sand with boulder	11	Medium dense coarse sand	22	Medium dense clayey Sand with gravel

15.5	100	Very dense fine sand with boulder and gravel	49	Dense coarse sand		
17	>50	Granite				
17.5			11	Medium dense sand	36	Medium dense Sand with gravel
17.55						
19.5			100	Very dense sand with gravel	60	Very dense sand with gravel
19.55	67	Dense sand with gravel				
23.5			100	Boulder and granite	21	Medium dense Sand with gravel
25.8	>50	Boulder				
27.5			54	Very dense sand with gravel		
27.55	100	Very dense sand with gravel and clay			31	Medium dense Sand with gravel
29.5	60	Very dense sand with gravel	83	Hard silt with gravel	50	very dense sand with gravel

2.4 Ground elevation profile

Fig. 6 shows the change in soil profile at Balaroa due to soil failure. The ground elevation profile before the earthquake was obtained from digital elevation model data [11]. As for the post-earthquake ground elevation profile, it was obtained through LIDAR data of the region. Due to the soil failure, the whole sandy topsoil layer between BH-01 and BH-02 slid and mounted at the lower elevation ground, as expressed in the figure in elevation at BH-03. Since the soil failure is predominant between BH-01 and BH-02, the current study focuses on the soil profile between BH-01 and BH-02.

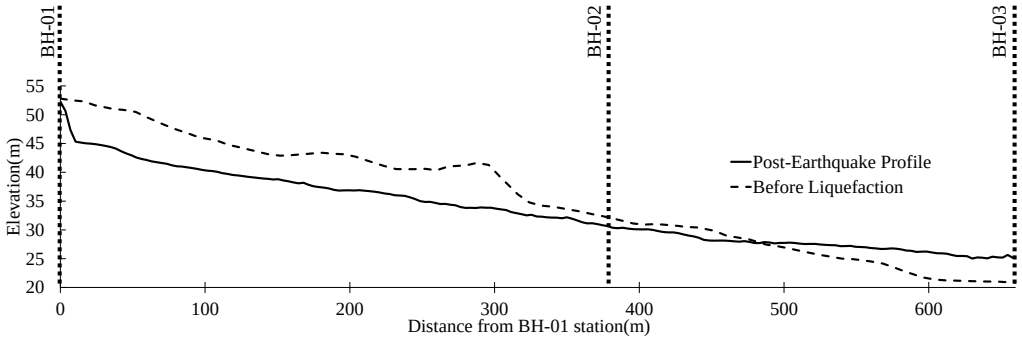

Fig. 6 Change in soil profile at Balaroa due to liquefaction

3. Soil Response; Frequency Characteristics

In order to understand the general frequency characteristics of the soil layer at BH-01 and BH-02, 1-D elastic soil response analysis is performed. The soil material properties are calculated from the boring data using conventional design method [10]. The detailed soil properties are discussed in the following section. Fig. 7 shows the Transfer Amplification function of the soil profile at BH-01 and BH-02, normalized to the maximum value. The first peak in the curves can be attributed to the soft topsoil. As the topsoil properties are different between BH-01 and BH-02 the peaks are at different frequencies (around 2.5Hz and 1.6 Hz). However, through observing the overlapping peak of amplification factor at the higher frequencies, it can be concluded that the soil properties at BH-01 and BH-02 below a certain depth are similar in related to increasing Vs by depth.

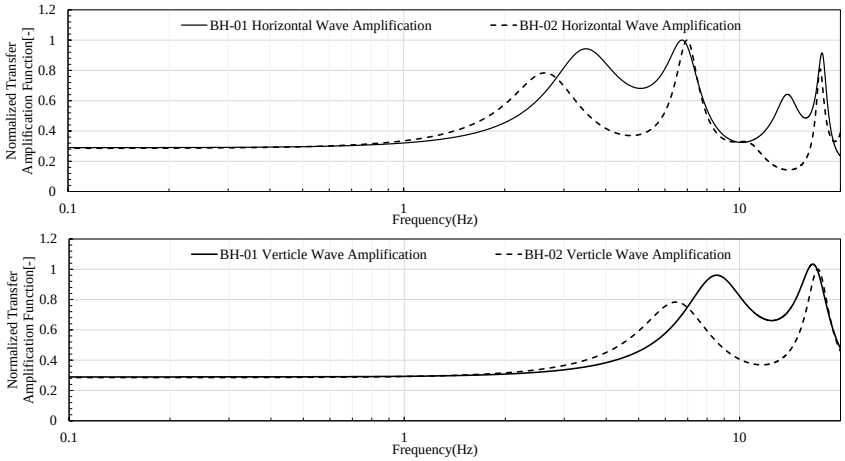

Fig. 7 Frequency characteristics of soil profile; Amplification Factor from engineering bedrock to surface

4. Numerical Simulation of Seismic Soil Response

4.1 Earthquake wave data processing

In order to understand the soil failure mechanism, equivalent linear dynamic analysis of the soil profile is performed. In the analysis, the earthquake wave is applied at the engineering bedrock level. In order to obtain the input earthquake wave for the current study, the wave is processed to obtain a realistic approach of the earthquake wave working on observed field. The earthquake wave process is as shown in Fig. 8. The recorded wave is first deconvoluted from the top surface to the engineering bedrock through 1-D soil response analysis, using soil material property at PCI-Palu station [10]. Once deconvoluted, rotational transformation is applied to the earthquake wave in order to obtain the input earthquake wave in the direction of the soil profile considered, viz., BH-01 to BH-02

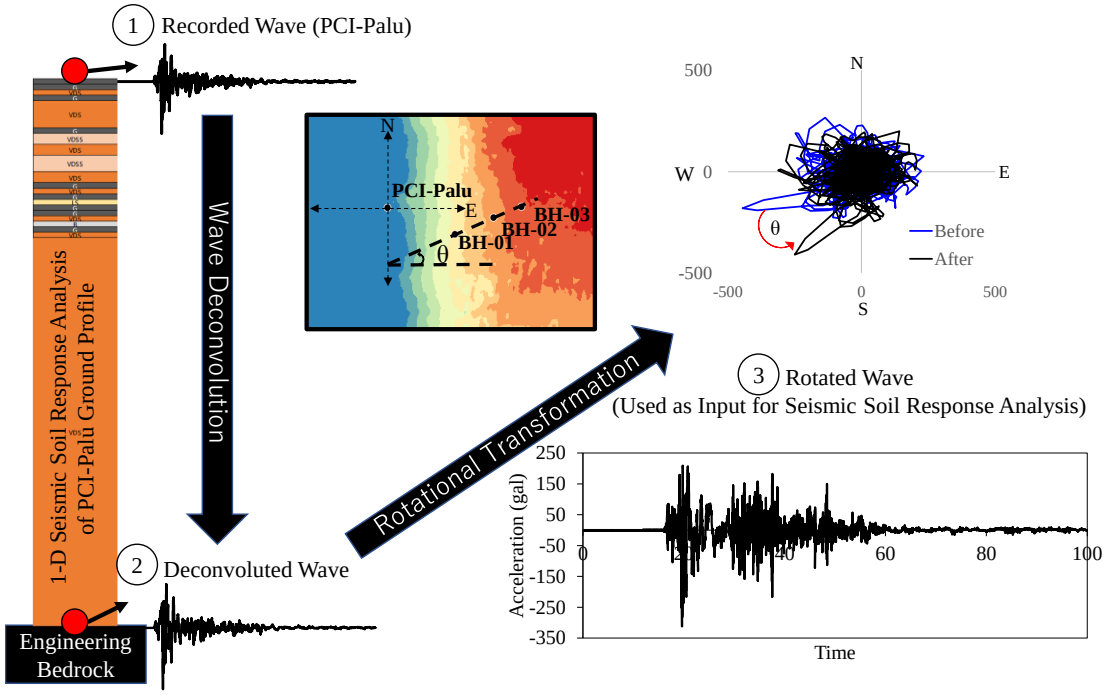

Fig. 8 Recorded earthquake wave processing performed in this study

4.2 1-D Seismic Soil Response Analysis

1-D seismic soil response analysis is performed using k-Shake, a frequency based equivalent linear soil response analysis program [4]. Table 2 lists the material properties used for the analysis. The nonlinear shear strain dependent material property curves are shown in Fig. 9. There is a requirement to perform analysis on soil profile before the earthquake, however only post-earthquake boring data is available. To overcome this problem, the material property of the topmost unknown layer of the soil model is assumed to be of the same material type as the topmost layer of the post-earthquake boring data. The soil profiles at BH-01 and BH-02 are analyzed separately for the horizontal input earthquake wave motion.

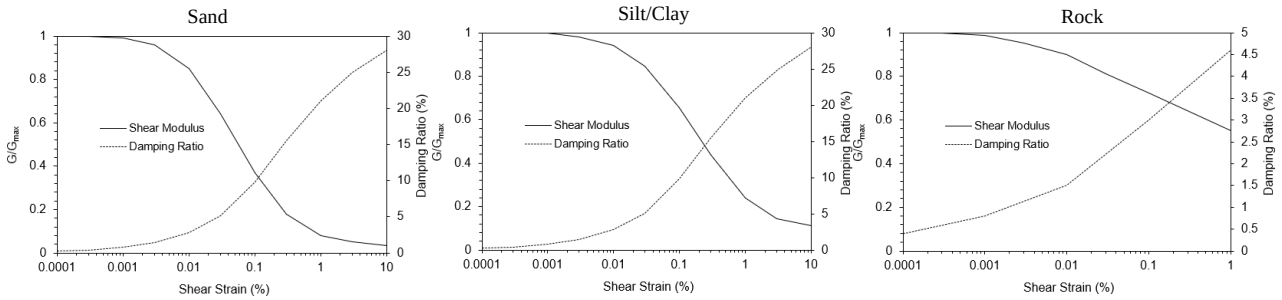

Fig. 9 Strain dependent non-linear material property used in soil response analysis

Table 2 – Soil Properties used for soil response analysis

Mat. No	Soil Classification	Weight Volume (kN/m3)	Vs (m/s)	Vp (m/s)	Elastic Modulus (kN/m2)	Shear Modulus (kN/m2)	Poisson ratio [-]
1	Very Loose Sand	17	100.79	246.89	4.93E+04	1.76E+04	0.4
2	Loose Sand	17	160.00	391.92	1.24E+05	4.44E+04	0.4
3		17	166.41	407.61	1.58E+05	2.80E+04	0.4
4		17	126.99	311.07	7.83E+04	2.80E+04	0.4
5	Medium stiff Silt	18	208.01	509.52	2.22E+05	7.94E+04	0.4
6	Hard Silt	20	385.52	944.33	8.49E+05	3.03E+05	0.4
7	Medium Dense Sand	20	213.47	522.90	2.60E+05	9.29E+04	0.4
8		20	188.11	460.77	2.02E+05	7.22E+04	0.4
9		20	177.92	435.81	1.81E+05	6.46E+04	0.4
10	Dense sand	21	389.10	953.09	9.08E+05	3.24E+05	0.4
11		21	292.74	717.08	5.14E+05	1.84E+05	0.4
12	Very Dense Sand	22	798.88	1956.87	4.01E+06	1.43E+06	0.4
13		22	519.49	1272.49	1.70E+06	6.05E+05	0.4
14		22	475.36	1164.40	1.42E+06	5.07E+05	0.4
15	Hard Silt	22	448.79	1099.32	1.27E+06	4.52E+05	0.4
16	Boulder	19	296.49	726.25	4.77E+05	1.70E+05	0.4
17		19	377.90	925.65	7.75E+05	2.77E+05	0.4
18		22	430.07	1053.46	1.16E+06	4.15E+05	0.4
19	Granite	22	430.07	1053.46	1.16E+06	4.15E+05	0.4

4.3 2-D Seismic Soil Response Analysis

In the present study, the SuperFLUSH/2D program [2] is used for 2-D soil analysis. The overall analysis flow is given in Fig. 10. Since a FEM model is used, it is necessary to simulate the semi-infinite soil at boundaries. Fig. 11 shows the boundary condition used in the current study, where energy transmitting boundary is applied. For the 2-D simulation it is assumed that the soil is stratified, and the stratification slope is obtained by matching similar soil types at BH-01 and BH-02 and joining them linearly. At locations where the soil strata are different the soil layers are assumed to exist only in one half of the model. The soil model used for simulation and the material classification of the elements can be seen in Fig. 12. For the 2-D simulation both the vertical and horizontal input earthquake wave are simultaneously applied.

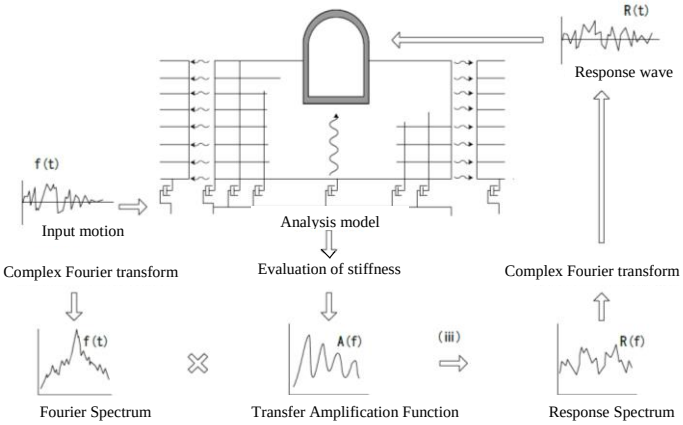

Fig. 10 Frequency response analysis flow in SuperFLUSH 2D

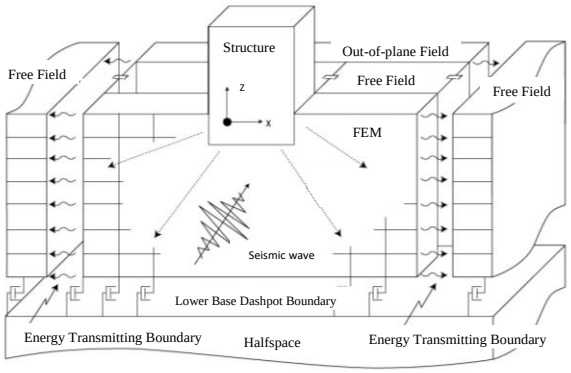

Fig. 11 Boundary conditions for analysis model

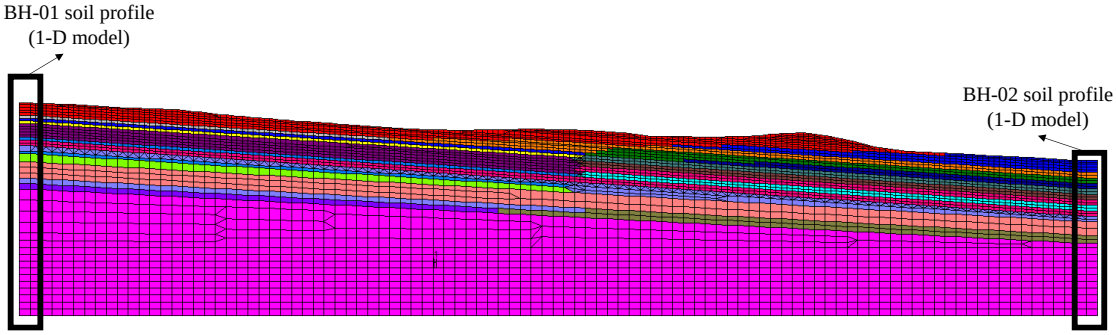

Fig. 12 Mesh used for 2-D soil response analysis

5. Liquefaction Analysis

5.1 Analysis details

Liquefaction analysis safety factor for the soil was calculated by the method suggested by Boulanger and Idriss [7][8]. The parameters used for the liquefaction safety factor calculation is given in Table 3.

Table 3 – Parameters used for liquefaction analysis

Earthquake Magnitude	7.5
Energy ratio correction factor (C_E)	0.8
Borehole diameter	89 mm
Borehole diameter correction factor (C_B)	1
Sampling method correction factor (C_S)	1
Fine content	5 %

For both the 1-D and 2-D analysis earthquake induced cyclic stress ratio (CSR) used in the liquefaction factor of safety calculation is directly obtained though soil response analysis given by the Eq. (1)

$$CSR = 0.65 \frac{\tau_{max}}{\sigma'_v} \tag{1}$$

where τmax = maximum earthquake induced shear stress obtained from soil response analysis, σ'v = vertical effective stress.

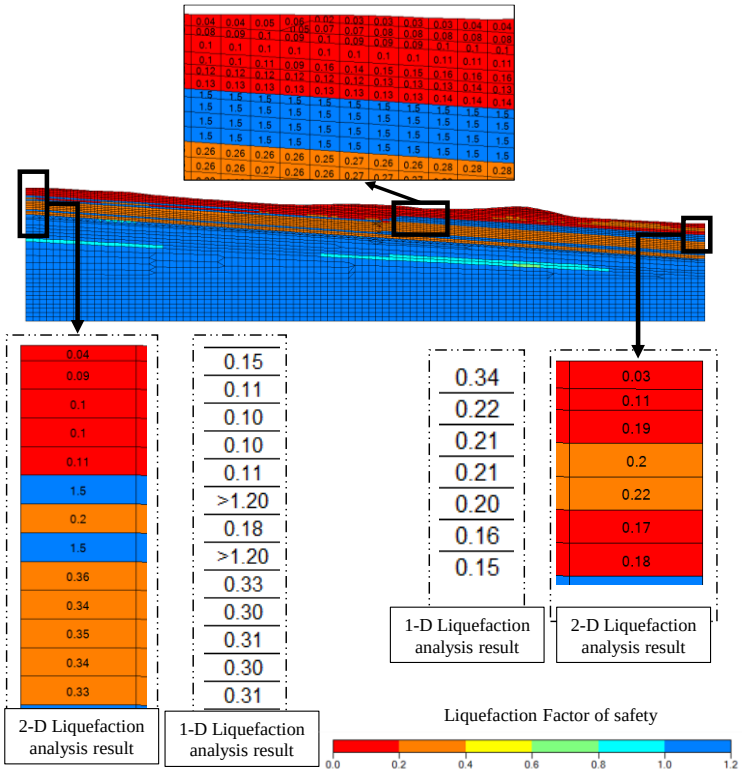

Fig. 13 Comparison of analysis results obtained from 1-D and 2-D soil response analysis

5.2 Analysis Results

The liquefaction results obtained from 1-D and 2-D analysis are compared in Fig. 13. The top layer of soil which comprises of very loose sand resulted in low factor of safety values. At a depth of around 6m from the top surface there is boulder and gravel at BH-01 and BH-02 respectively. This leads a clear demarcation at both BH-01 and BH-02, that up to a particular depth the soil was highly susceptible to liquefaction failure. Similar results were obtained both from 1-D analysis and 2-D analysis, however the 2-D analysis leads to slightly more critical factor of safety values. This can be attributed to the consideration of the vertical wave motion which, in the case of the Sulawesi earthquake had a larger PGA compared to the horizontal wave motion.

In order to verify the analysis results, Fig. 14 shows the overlay of the liquefaction contour and the post-earthquake ground profile. The region in the model where the factor of safety is <0.2 correlates well with the soil failure profile. The failure of the soil surface can be mainly attributed due to liquefaction. The results also justify the soil layer stratification assumption made during modelling.

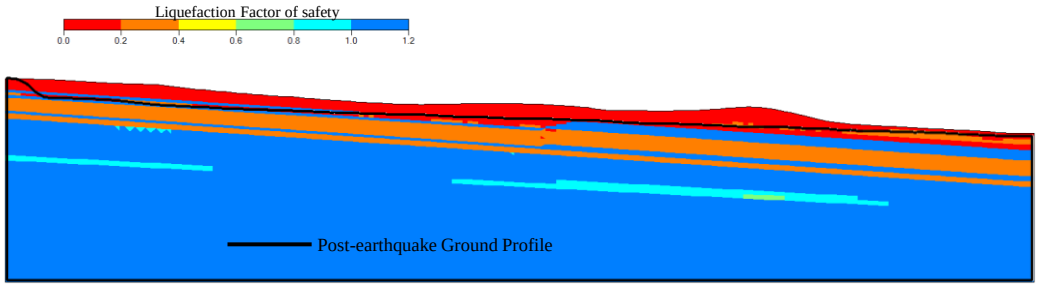

Fig. 14 Comparison of analysis result and the observed post-earthquake soil profile

6. Slope Stability Analysis

6.1 Analysis model

The most critical slope of the entire model is selected, and slope stability analysis is executed on POST-S program [3] by combining static analysis and dynamic analysis result. Below parameter are being used for the calculation, obtained through N-SPT correlation soil properties [12],[13]. The observed slope soil layer is assumed as sands and silt layers as described in Table 4 and previous section. The safety factor is calculated by comparing resistance and working shear stress (expressed through Mohr-Coulomb) on the elements passed by the slip lines. The residual deformation is calculated once the safety factor < 1.00 using Newmark method.

Table 4 – Parameter used for Slope Stability Analysis

Material No	Material properties	Friction Angle (°)	Cohesion (kPa)
1	Very Loose Sand	25	-
2	Loose Sand 1	30	-
3	Loose Sand 2	30	-
4	Loose Sand 3	25	-
5	Medium Stiff Silt	-	50
6	Hard Stiff Silt	-	200

6.2 Analysis Results

Several slip lines are defined considering the soil type and failure locations as described in Fig. 15. Finally, 3 slip lines with lowest safety factor are selected. The lowest safety factor occurred on Slip 2 which consist of sandy soil and located at the top of the slope as described in Table 5. The elements observed on Slip 2 consist of very loose sand with low shear strength and located on the top of the slope, resulting to lowest shear resistance. Nevertheless, the lowest safety factor does not go below 1.00.

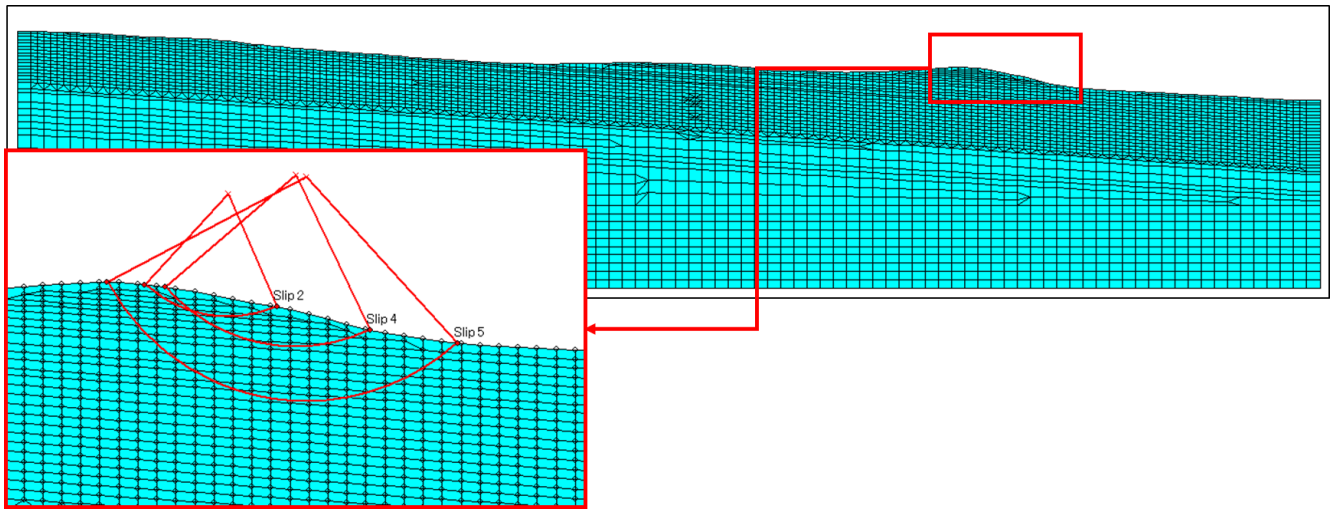

Fig. 15 Selected Slip Surface for Slope Stability Analysis

Table 5 – Slip Minimum Safety Factor

Slip no.	Safety Factor
Slip 2	1.04
Slip 4	1.26
Slip 5	1.41

7. Conclusion

The current study shows the predominance of liquefaction in the soil failure mechanism at Balaroa during the 2018 Sulawesi earthquake. From the liquefaction analysis of the soil, shows that the soil slope was highly susceptible to liquefaction even before the earthquake occurred. Although the current study performs soil response analysis with limited data points, good correlation between the calculated liquefaction failure profile and actual earthquake soil failure profile was obtained. Performing 2-D simulations helps in understanding the global failure mechanism, while considering both horizontal and vertical wave motions. It provides a balanced option when compared to the simple 1-D soil modelling methods.

Various factors that contributed to the soil failure at Balaroa, Palu are examined through the current study. From the slope stability analysis, it was evident that influence of slope failure in the global failure mechanism was minimal. Thus, it is concluded that despite the existing of slope on the site, the main factor of the soil failure in Balaroa is due to liquefaction. This paper provides even more evident for the future disaster mitigation against liquefaction for Palu region that might still prone to it.

8. Acknowledgements

This study would not be able to be completed without the support of Mr. Lutfi Faizal of The National Center for Earhquake Studies of Indonesia (PuSGeN) and Mr. Sigit Pramono of Indonesia Meteorological, Climatological, and Geophysical Agency (BMKG).

9. References

[1] Irsyam, M., Sahadewa, A., Hanifa R., Harninto, D. S., Muntohar, A, Djarwadi, D., Prakoso, W, Natawi-jaya, D.H., Latief, H., Asrurifak, M., Faisal, L., Pramono S., Daryono, M., & Nazir, R. 2018. Palu Earthquake 2018, A Preliminary Geotechnical Engineering Report. *JICA Project Development of Regional Disaster Risk Resilience Plan in Central Sulawesi*, Tokyo. 27th April 2019.

[2] Kozo Keikaku Engineering Inc and Jishin Kougaku Kenkyusyo Inc. "SuperFLUSH/2D ver6.0 manual".

[3] Kozo Keikaku Engineering Inc and Jishin Kougaku Kenkyusyo Inc. "POST-S for Windows ver.1.1 User Manual".

[4] Kozo Keikaku Engineering Inc and Jishin Kougaku Kenkyusyo Inc. "k-SHAKE+ for Windows ver.6.1 User Manual"

[5] Sahadewa, A., Irsyam, M., Hanifa, R., Mikhail, R., Pamumpuni, A., Nazir, R., et al. Overview of the 2018 Palu Earthquake. *7th International Conference on Earthquake Geotechnical Engineering*, Rome, 857–869. 2019

[6] JICA-BMKG. Ground motion due to the 2018 Palu earthquake record. PCI Palu Station, 2018.

[7] Idriss, I.M., Boulanger, R.W. Soil Liquefaction during Earthquakes. *Earthquake Engineering Research Institute (EERI)*. Oakland, California, USA 2008.

[8] Idriss, I.M., Boulanger, R.W. SPT-Based Liquefaction Triggering Procedures. Davis, California. 2010.

[9] USGS. *https://earthquake.usgs.gov/earthquakes/eventpage/us1000h3p4/shakemap/pga*

[10] JICA, PT Geomarindex. Geotechnical Investigation Landslide Area-2. *Project for Development of Regional Disaster risk Resilience Plan in Central Sulawesi*. August 2019.

[11] Indonesia Geospatial Information Agency. *http://tides.big.go.id/DEMNAS/*

[12] Karol, R.H. Soils and Soil Engineering. Prentice-Hall, 1960

[13] Meyerhof, G.G. Penetration Tests and Bearing Capacity of Cohesionless Soil. *Journal of the Soil Mechanics and Foundations Division*. 1956. Vol. 82, Issue 1, 1-19.

